Asian Winter Monsoon Summary for 2011/2012

Many parts of East and Central Asia experienced significantly below-normal temperatures throughout winter (December – February) 2011/2012. This report summarizes the related surface climate characteristics, atmospheric circulation and primary factors contributing to the cold conditions observed. The relevant factors were clarified based on investigation by JMA's Advisory Panel on Extreme Climate Events.

Note: JRA/JCDAS (Onogi et al. 2007) atmospheric circulation data and COBE-SST (JMA 2006) sea surface temperature (SST)/sea ice concentration data were used for this investigation. The outgoing longwave radiation (OLR) data referenced to infer tropical convective activity were originally provided by NOAA. The base period for the normal is 1981 – 2010.

1. Surface climate conditions

In winter 2011/2012, Asian countries in the mid-latitudes experienced significantly lower-than-normal temperatures due to strong cold-air inflow, while the northern part of Siberia and southern Asian countries experienced higher-than-normal temperatures (Figure 1.1).

Figure 1.2 shows extreme climate events that occurred from December 2011 to February 2012. In December 2011, extremely low temperatures were observed in eastern Mongolia and southern Central Asia, while extremely high temperatures were seen from northern Central Siberia to northern Western Siberia. In January, extremely low temperatures were observed around Mongolia, and extremely light precipitation amounts (snow) were seen from the southern part of Western Siberia to Kazakhstan. In February, extremely low temperatures were observed from central Mongolia to the Middle East, while extremely high temperatures were seen from northern Central Siberia to northern Western Siberia. Extremely light precipitation (snow) amounts were observed from Western Siberia to northern Kazakhstan.

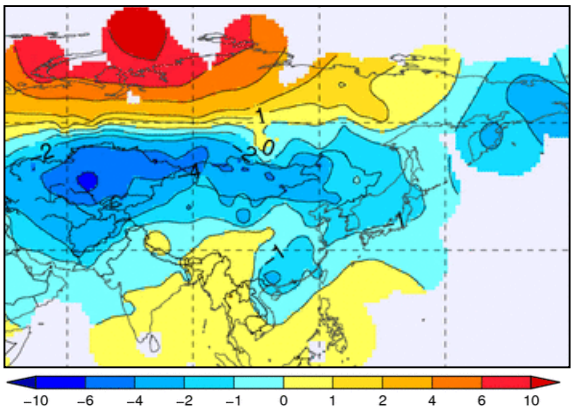

Figure 1.1 Seasonal temperature anomalies for winter (December – February) 2011/2012
Anomalies are deviations from the normal (i.e., the 1981 – 2010 average). The contour interval is 1°C.

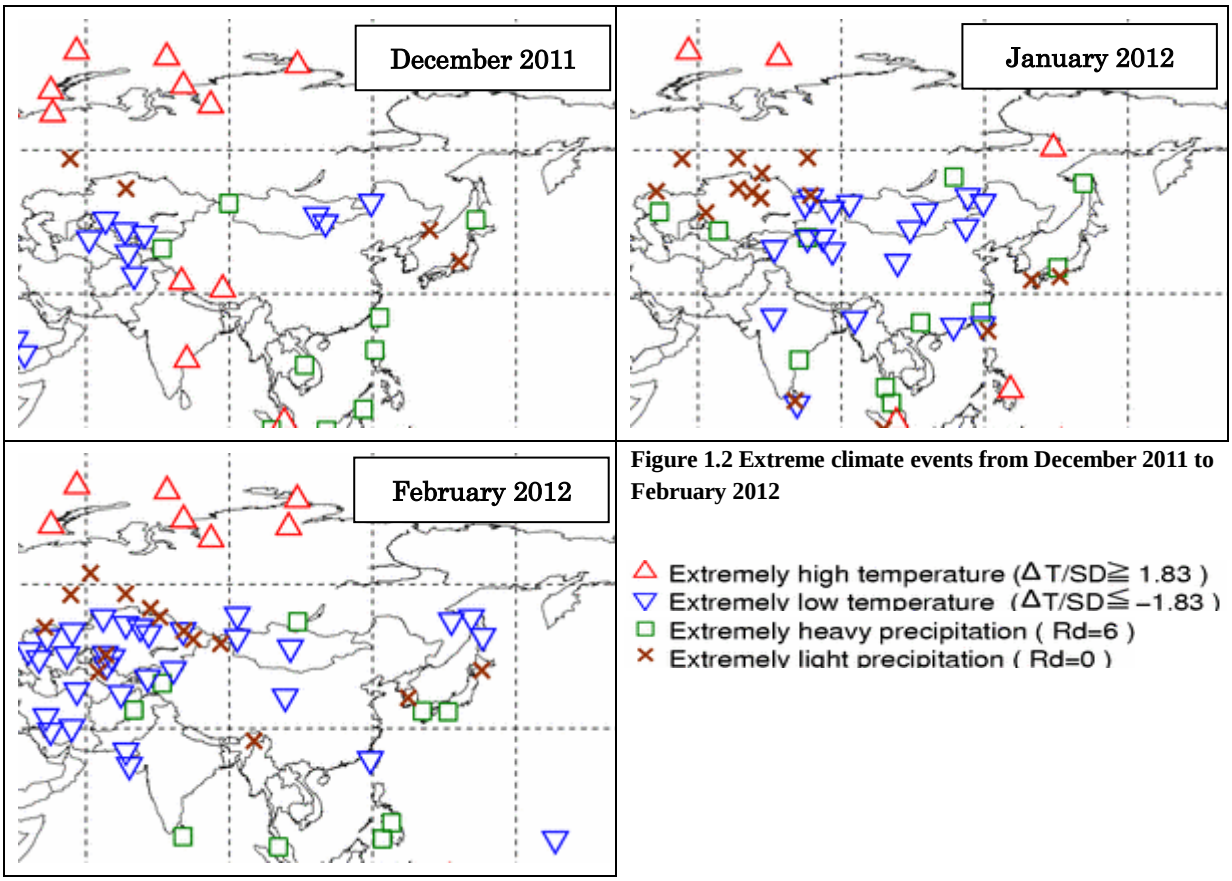

Figure 1.2 Extreme climate events from December 2011 to February 2012

2. Characteristic atmospheric circulation causing the cold winter conditions

In the 500-hPa height field for boreal winter 2011/2012 (Figure 2.1 (a)), distinct wave trains were observed from the North Atlantic to Eurasia with positive anomalies over western Siberia and negative anomalies over northeastern Asia, indicating significant meandering of the polar front jet stream. This wavy pattern persisted throughout the winter (Figure 2.2), forming in association with stationary Rossby wave packets propagating eastward from the North Atlantic (Figure 2.3).

In the sea level pressure field (Figure 2.1 (b)), positive anomalies were seen across northern Eurasia, and especially over western Siberia. The Siberian High was significantly enhanced and expanded, reaching its strongest level since 1979/1980 (Figure 2.4). The intensification of the Siberian High was associated with upper-level ridges over western Siberia (Takaya and Nakamura 2005a and 2005b) (Figure 2.5). The enhanced Siberian High contributed to an intensification of the East Asian winter monsoon, which strengthened cold air advection over the region.

In the 850-hPa temperature field (Figure 2.1 (c)), negative anomalies were seen in the mid-latitudes of Eurasia, especially over Central and East Asia. In the lower troposphere, anticyclonic circulation anomalies centered over western Siberia brought a cold air mass from central and eastern Siberia to Central Asia and Mongolia, contributing to extremely below-normal temperatures in the latter areas and enhancing the Siberian High (Figure 2.6). Anticyclonic circulation anomalies over western Siberia were associated with the upper-level blocking ridges there.

In the upper troposphere, Rossby wave packets propagated eastward from southern China to the area east of Japan (Figure 2.3). Distinct anticyclonic circulation anomalies were seen over the former area and cyclonic circulation anomalies were observed over the latter. In line with these conditions, northerly

wind anomalies were seen over Japan, indicating a southward meandering of the subtropical jet stream around the country (Figure 2.7). In association, upper-level cold air frequently moved into Japan, contributing to below-normal temperatures over the country and heavy snowfall on its Sea of Japan side.

In the zonally averaged fields over the mid-latitudes from central to eastern Eurasia, temperatures were below normal throughout the whole of the troposphere, and geopotential heights were below and above normal in the upper and lower troposphere, respectively (Figure 2.8).

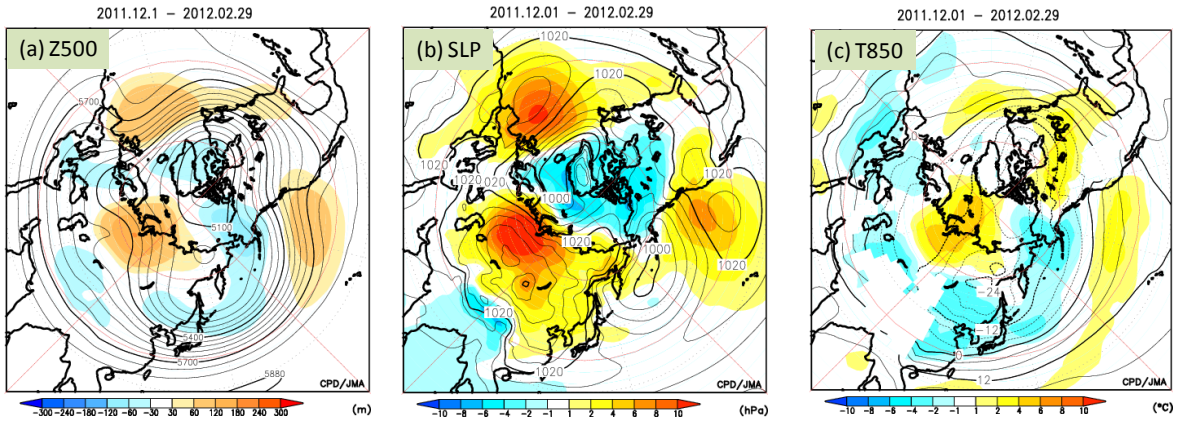

Figure 2.1 Three-month mean (a) 500-hPa height, (b) sea level pressure and (c) 850-hPa temperature for December 2011 – February 2012

The contour intervals are (a) 60 m, (b) 4 hPa and (c) 4˚C. The shading indicates respective anomalies (i.e., deviations from the 1981 – 2010 average). Contours/shading are not shown for areas with altitudes exceeding 1,600 m.

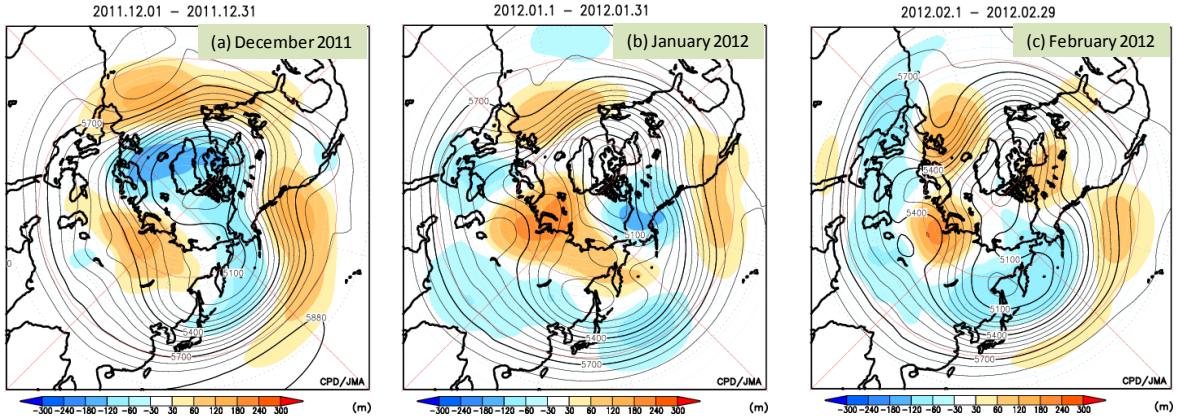

Figure 2.2 Monthly mean 500-hPa height for December 2011 (a), January 2012 (b) and February 2012 (c)

The contour intervals are 60 m, and the shading indicates 500-hPa height anomalies.

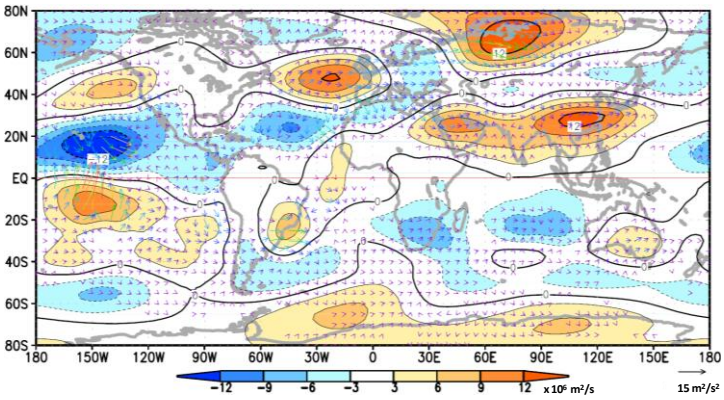

Figure 2.3 Three-month mean 200-hPa stream function anomalies and wave activity flux for December 2011 – February 2012

The contours and shading indicate stream function anomalies at intervals of 3×10^6 m^2/s. The warm- (cold)-color shading denotes anticyclonic (cyclonic) circulation anomalies in the Northern Hemisphere, and vice versa in the Southern Hemisphere. The vectors show wave activity flux (unit: m^2/s^2) based on Takaya and Nakamura (2001).

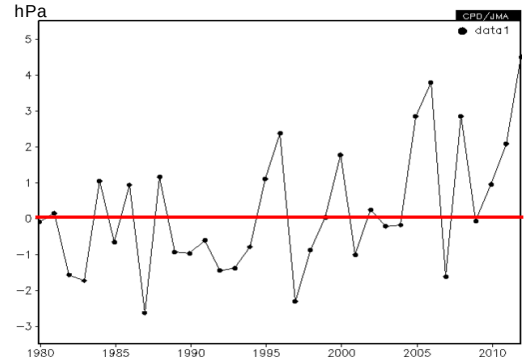

Figure 2.4 Interannual variation of area-averaged sea level pressure anomalies (unit: hPa) around the center of the Siberian High (40˚N – 60˚N, 80˚E – 120˚E) for winters (December – February) from 1979/1980 to 2011/2012

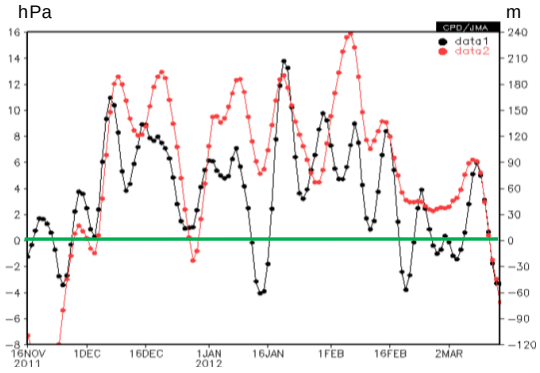

Figure 2.5 Time series of area-averaged sea level pressure anomalies around the center of the Siberian High (40˚N – 60˚N, 80˚E – 120˚E) and area-averaged 500-hPa height anomalies over western Siberia (50˚N – 70˚N, 60˚E – 90˚E) from 16 November, 2011, to 15 March, 2012

The black and red lines indicate five-day running mean values of area-averaged sea level pressure anomalies (unit: hPa) and 500-hPa height anomalies (unit: m), respectively. The coefficient of correlation between them for the period from 1 December, 2011, to 29 February, 2012, is 0.60 (with a 95% confidence level).

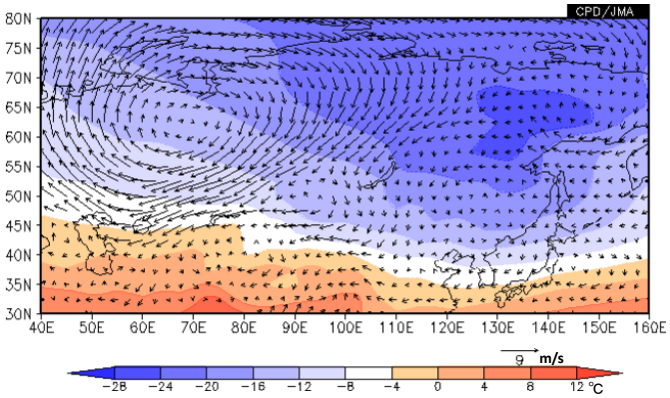

Figure 2.6 Three-month mean 850-hPa wind vector anomalies and 850-hPa normal temperatures for December 2011 – February 2012

The vectors indicate wind vector anomalies (unit: m/s), and the shading denotes normal temperatures (unit: ˚C; 1981 – 2010 average).

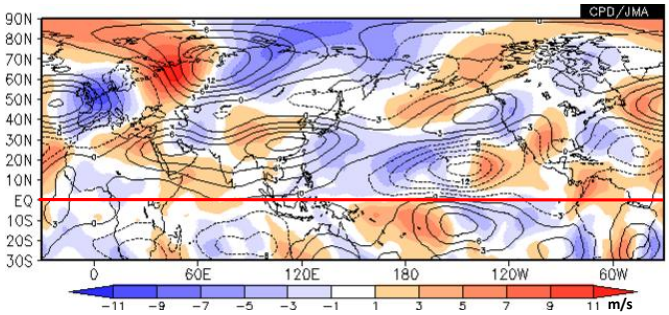

Figure 2.7 Three-month mean 200-hPa stream function anomalies and meridional wind anomalies for December 2011 – February 2012
The contours denote stream function anomalies at intervals of 3×10^6 m^2/s. The shading indicates meridional wind anomalies (unit: m/s), and positive (warm color) and negative (cold color) values denote southerly (northerly) wind anomalies, respectively.

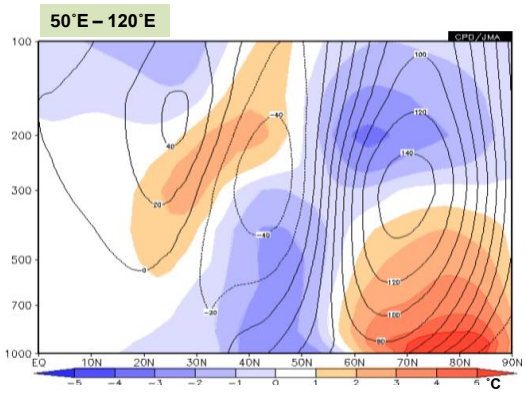

Figure 2.8 Latitude-height cross section of three-month mean geopotential height anomalies and temperature anomalies zonally averaged between 50˚E – 120˚E for December 2011 – February 2012
The contours denote geopotential height anomalies at intervals of 20 m. The shading indicates temperature anomalies (unit: ˚C).

3. Primary factors

3.1 Southward meandering of the subtropical jet stream around Japan

In winter 2011/2012, SST anomaly patterns in the Pacific exhibited La Niña-like conditions* (Figure 3.1 (a)), and convective activity was enhanced around the Maritime Continent throughout the season (Figure 3.1 (b)). It can be inferred that this active convection led to the upper-level anticyclonic circulation anomalies seen around southern China by forcing a Gill-type response (Gill 1980) (Figure 3.1 (b)). These anomaly patterns in convective activity and atmospheric circulation are typical of past La Niña events (Figure 3.2). Accordingly, the southward meandering of the subtropical jet stream around Japan, which caused frequent cold air flows over the country, was considered to be associated with the La Niña-like conditions.

* JMA defines a La Niña event as a phenomenon in which the five-month running-mean values of monthly SST deviations from the sliding 30-year mean for the El Niño monitoring region (NINO.3: 5˚S – 5˚N, 150˚W – 90˚W) stay at -0.5˚C or below for six consecutive months or longer. As SST values remained below -0.5˚C for only five consecutive months from September 2011 to January 2012, the criteria for JMA's La Niña definition were not met.

3.2 Significant meandering of the polar front jet stream over Eurasia

The wave trains along the polar jet stream over Eurasia that contributed to the intensification and northwestward expansion of the Siberian High mainly originated in the North Atlantic, where upper-level cyclonic and anticyclonic circulation anomalies were seen over subtropical and mid-latitude areas, respectively (Figure 2.3).

In past La Niña events (Figure 3.2), anticyclonic circulation anomalies tended to appear across the

middle latitudes from the eastern North Pacific to the North Atlantic with three centers west of the USA, over southeastern parts of the country, and west of Europe. Related circulation anomalies for winter 2011/2012 (Figure 2.3) showed anomaly patterns typical of past events. Thus, La Niña-like conditions may be associated with the anticyclonic circulation anomalies observed in the North Atlantic mid-latitudes.

Significant divergence anomalies in the upper troposphere were seen around northern South America and the tropical North Atlantic in association with the enhanced convective activity observed there (Figure 3.3). Anomalous northward-flowing divergent winds seen on the northern side of the divergence converged over areas east of the Caribbean Sea where the Rossby wave source (Sardeshmukh and Hoskins 1988) exhibited positive values (indicating vorticity sources) (Figure 3.4). Active convection around northern South America and the tropical North Atlantic was therefore considered responsible for the generation of upper-level cyclonic circulation anomalies as an origin of the wave trains seen over the subtropical North Atlantic.

Active convection around northern South America and the tropical North Atlantic was also seen in past La Niña events (Figure 3.2 (a)). SSTs were above normal in northwestern parts of the tropical North Atlantic and significantly below normal in the tropical South Atlantic (Figure 3.1). Statistical analysis shows that convective activity over tropical areas tends to be enhanced when tropical SSTs are below normal in the tropical South Atlantic (Figure 3.5) and when dipole SST anomaly patterns with positive north and negative south values are seen in the tropical Atlantic (Figure 3.6).

Accordingly, it can be inferred that the SST anomalies observed in the tropical Atlantic and the La Niña-like conditions seen contributed to anomalous atmospheric circulation over the North Atlantic, thereby inducing eastward-stretching wave trains.

3.3 Low temperatures across the Eurasian mid-latitudes

In past La Niña periods, a tendency has been observed in the Eurasian mid-latitudes whereby temperatures in the troposphere and geopotential heights in the upper troposphere are lower than normal (without a 90% confidence level) (Figure 3.7). The related anomalies for winter 2011/2012 (Figures 2.1 and 2.8) echo this tendency. Steady response to diabatic heating anomalies around the Maritime Continent was examined using a linear baroclinic model (LBM; Watanabe and Kimoto 2000). The LBM results (Figure 3.8) indicated that both lower-level temperatures and upper-level height were below normal in the mid-latitudes of Eurasia, which was consistent with characteristics seen in past La Niña events. Accordingly, the La Niña-like conditions observed may be responsible for low temperatures in the Eurasian middle latitudes.

3.4 Arctic sea ice

During winter 2011/2012, the sea ice extent in the Arctic Ocean, especially in the Barents Sea and the Kara Sea, remained far below the 1979 – 2000 average (Figure 3.9). According to statistical analysis (Figure 3.10), atmospheric circulation anomalies over Eurasia seen in light sea ice around the seas echoed related anomalies observed during the winter (Figure 2.1). Recent studies (e.g., Honda et al. 2009, Inoue et al. 2012) have reported that a reduction in the amount of floating sea ice tends to induce amplification of the Siberian High, leading to cold anomalies in East Asia. Thus, the light sea ice observed around the Barents Sea and the Kara Sea may contribute to the enhancement of the Siberian High.

4. Summary

In the 2011/2012 Asian winter monsoon season, Central and East Asia experienced cold winter conditions due to a strong Siberian High and frequent cold surges. The possible primary factors contributing to these conditions are summarized in Figure 4.1, but the related mechanisms have not yet been fully clarified.

References

Gill, A. E., 1980: Some simple solutions for heat-induced tropical circulation. *Quart. J. Roy. Meteor. Soc.*, **106**, 447 – 462.

Honda, M., J. Inoue, and S. Yamane, 2009: Influence of low Arctic sea-ice minima on anomalously cold Eurasian winters. *Geophys. Res. Lett.*, **36**, L08707, doi: 10.1029/2008GL037079.

Inoue, J., M. Hori, and K. Takaya, 2012: The Role of Barents Sea Ice in the Wintertime Cyclone Track and Emergence of a Warm-Arctic Cold-Siberian Anomaly. *J. Climate*, **25**, 2561 – 2568.

JMA, 2006: Characteristics of Global Sea Surface Temperature Data (COBE-SST). *Monthly Report on Climate System*, Separated Volume No. **12**.

Onogi, K., J. Tsutsui, H. Koide, M. Sakamoto, S. Kobayashi, H. Hatsushika, T. Matsumoto, N. Yamazaki, H. Kamahori, K. Takahashi, S. Kadokura, K. Wada, K. Kato, R. Oyama, T. Ose, N. Mannoji and R. Taira, 2007: The JRA-25 Reanalysis. *J. Meteorol. Soc. Japan*, **85**, 369 – 432.

Sardeshmukh, P. D., and B. J. Hoskins, 1988: The generation of global rotational flow by steady idealized tropical divergence. *J. Atmos. Sci.*, **45**, 1228 – 1251.

Takaya, K., and H. Nakamura, 2001: A formulation of a phase-independent wave-activity flux for stationary and migratory quasigeostrophic eddies on a zonally varying basic flow. *J. Atom. Sci.*, **58**, 608 – 627.

—, and —, 2005a: Mechanisms of intraseasonal amplification of the cold Siberian high. *J. Atmos. Sci.*, **62**, 4423 – 4440.

—, and —, 2005b: Geographical dependence of upper-level blocking formation associated with intraseasonal amplification of the Siberian high. *J. Atmos. Sci.*, **62**, 4441 – 4449.

Watanabe, M., and M. Kimoto, 2000: Atmospheric-ocean thermal coupling in North Atlantic: Apositive feedback, *Quart. J. R. Met. Soc.*, **126**, 3343 – 3369.

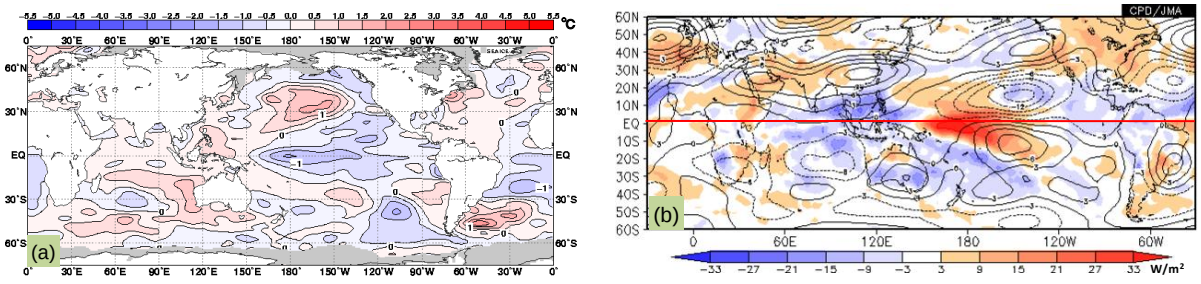

Figure 3.1 Three-month mean (a) sea surface temperature (SST) anomalies and (b) 200-hPa stream function anomalies and outgoing longwave radiation (OLR) anomalies for December 2011 – February 2012

(a) The contours and shading indicate SST anomalies at intervals of 0.5˚C. (b) The contours denote stream function anomalies at intervals of 3×10^6 m^2/s, and the shading indicates OLR anomalies (unit: W/m^2). The cold- (warm-) color shading denotes enhanced (suppressed) convective activity.

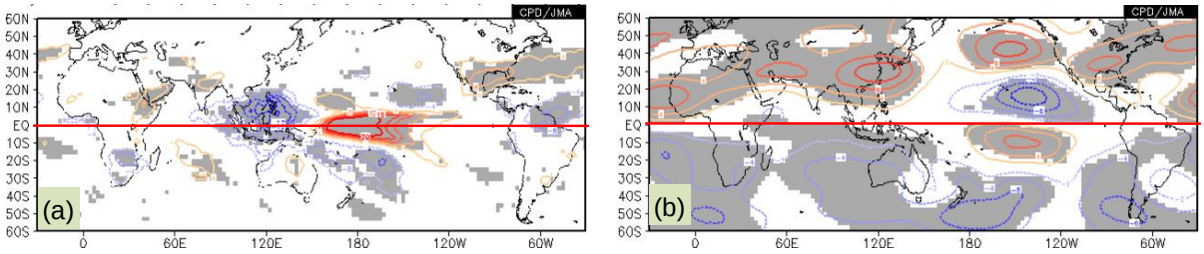

Figure 3.2 La Niña composites of three-month mean (a) outgoing longwave radiation (OLR) anomalies and (b) 200-hPa stream function anomalies for December – February

(a) The contours indicate OLR anomalies at intervals of 4 W/m^2 (shown between -20 W/m^2 and 20 W/m^2). (b) The contours denote stream function anomalies at intervals of 3 × 10^6 m^2/s. (a) and (b) The past La Niña winters (December – February) selected for the composites are those of 1984/1985, 1988/1989, 1995/1996, 1998/1999, 1999/2000, 2005/2006 and 2007/2008. The gray shading indicates a 95% confidence level as indicated by t-testing.

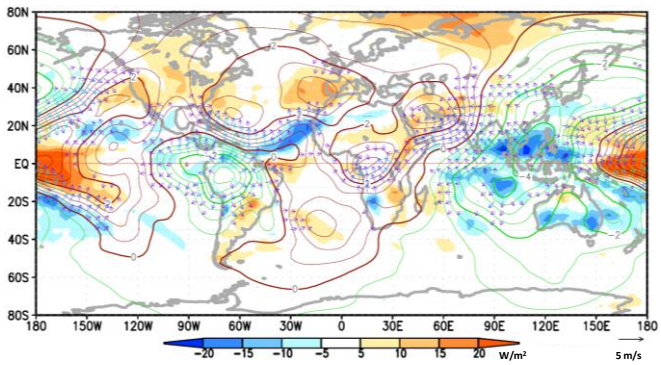

Figure 3.3 Three-month mean 200-hPa velocity potential anomalies, 200-hPa divergent wind anomalies and outgoing longwave radiation (OLR) anomalies for December 2011 – February 2012

The contours indicate velocity potential anomalies at intervals of 0.5 × 10^6 m^2/s. The vectors denote divergent wind anomalies (unit: m/s). The shading indicates OLR anomalies (unit: W/m^2). The cold-(warm-) color shading denotes enhanced (suppressed) convective activity.

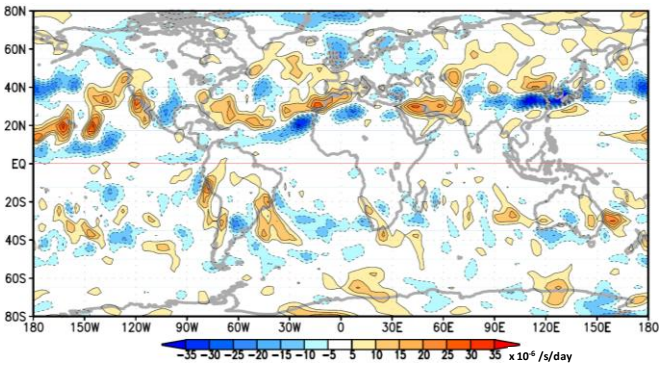

Figure 3.4 Rossby wave source anomalies at 200 hPa for December 2011 – February 2012

The contours and shading indicate Rossby wave source anomalies (unit: 5 × 10^{-6} /s/day). Positive (warm-color) and negative (cold-color) anomalies represent vorticity sources and sinks, respectively.

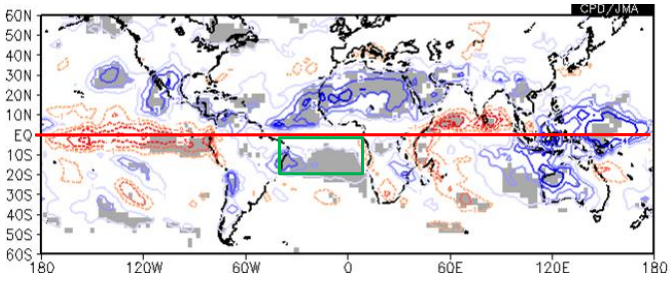

Figure 3.5 Three-month mean outgoing longwave radiation regressed onto area-averaged sea surface temperatures (unit: ˚C) in the tropical South Atlantic (green rectangle: 20˚S – eq., 40˚W – 10˚E) for winters (December – February) from 1979/1980 to 2010/2011

The contour intervals are 1 W/m^2, and positive and negative values are colored in blue and red, respectively. The gray shading indicates a 95% confidence level as indicated by t-testing.

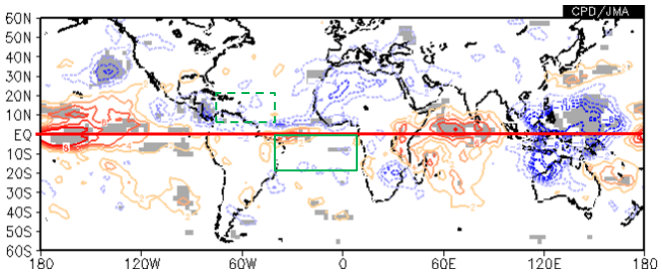

Figure 3.6 Composite of three-month mean outgoing longwave radiation anomalies for winter (December – February) when tropical sea surface temperatures were positive in the northwestern North Atlantic (dashed green rectangle: 5˚N – 20˚N, 75˚W – 40˚W) and negative in the South Atlantic (solid green rectangle: 20˚S – eq., 40˚W – 10˚E)

The winters selected for the composite are 1979/1980, 1980/1981, 1995/1996, 1996/1997, 2001/2002 and 2005/2006. The contour intervals are 2 W/m^2. The gray shading indicates a 95% confidence level as indicated by t-testing.

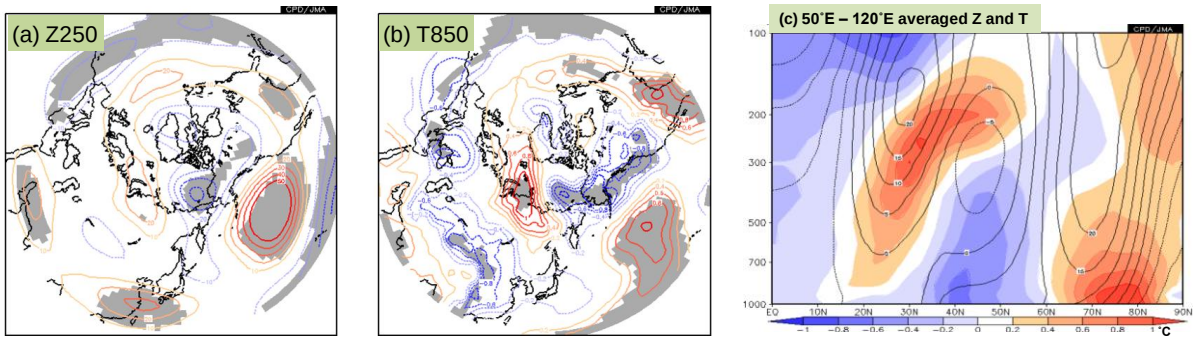

Figure 3.7 La Niña composites of three-month mean (a) 250-hPa height anomalies, (b) 850-hPa temperature anomalies, and (c) zonally-averaged geopotential height and temperature anomalies (50˚E – 120˚E) for winter (December – February)

(a) The contours indicate height anomalies at intervals of 10 m (shown between -50 m and 50 m). (b) The contours denote temperature anomalies at intervals of 0.2˚C (shown between -1˚C and 1˚C). (c) The contours denote geopotential height anomalies at intervals of 5 m, and the shading indicates temperature anomalies (unit: ˚C). (a) – (c) The past La Niña winters selected for the composites are those of 1984/1985, 1988/1989, 1995/1996, 1998/1999, 1999/2000, 2005/2006 and 2007/2008. The gray shading indicates a 90% confidence level as indicated by t-testing.

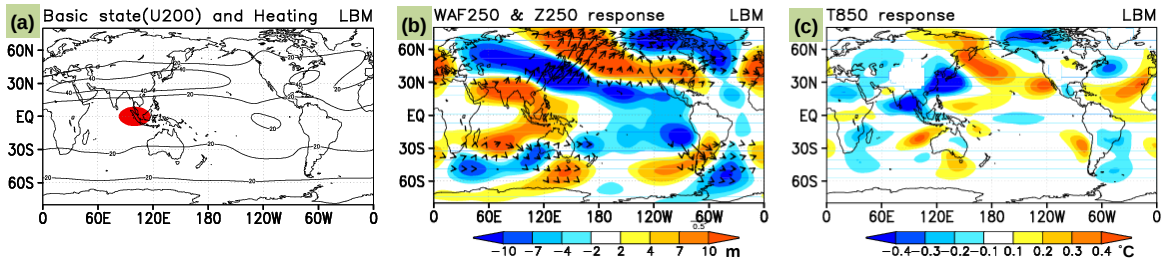

Figure 3.8 Steady response in a linear baroclinic model (LBM) to heating anomalies near the Maritime Continent

(a) The red ellipse indicates diabatic heating for the LBM with the basic state for January (i.e., the 1979 – 2004 average based on JRA-25 data). (b) The shading denotes the steady response of 250-hPa height anomalies (unit: m), and the vectors indicate wave activity fluxes (unit: m^2/s^2). (c) The shading indicates the steady response of 850-hPa temperature anomalies (unit: ˚C). (b) and (c) These anomalies as responses represent deviations from the respective basic states and are additionally subtracted from the zonal averages of the respective anomalies. The related steady responses to heating in the basic state for December and February (not shown) are similar to those for January.

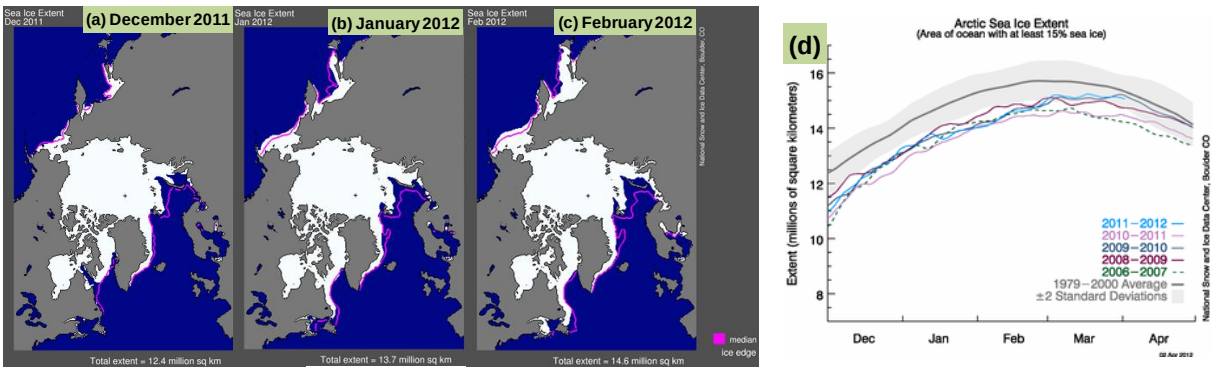

Figure 3.9 Arctic sea ice extent for winter 2011/2012

(a) – (c) Monthly Arctic sea ice extent for (a) December 2011, (b) January 2012 and (c) February 2012. The magenta line shows the 1979 to 2000 median extent for that month. The black cross marks the geographic North Pole. (d) Daily Arctic sea ice extent as of April 2, 2012, along with the corresponding values for the previous four years. The current year is shown in light blue, 2010 – 2011 in pink, 2009 – 2010 in dark blue, 2008 – 2009 in purple, and 2006 – 2007 (the year in which the record minimum was seen) in dashed green. The gray area around the average line shows the two-standard-deviation range of the data.

(Sources: National Snow and Ice Data Center (NSIDC), USA, at http://nsidc.org/arcticseaicenews/)

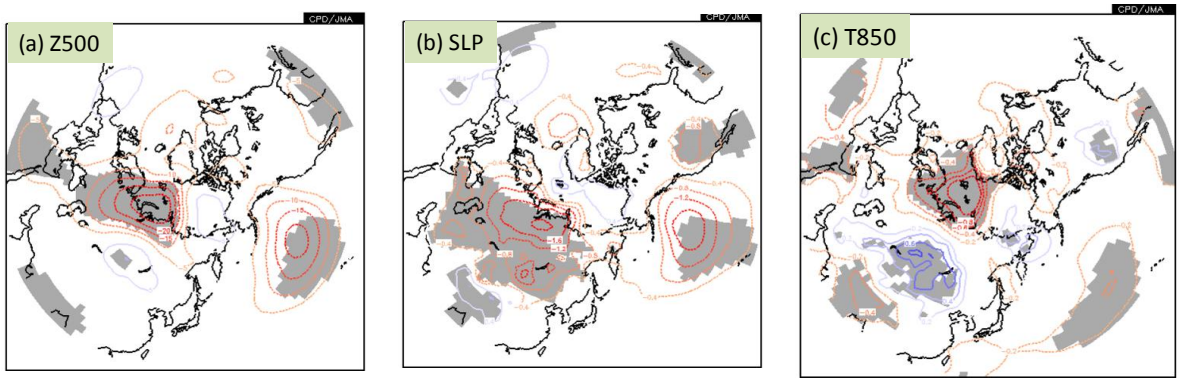

Figure 3.10 Three-month mean (a) 500-hPa height, (b) sea level pressure and (c) 850-hPa temperature regressed onto area-averaged sea ice extents around the Barents Sea and the Kara Sea (70˚N – 80˚N, 45˚E – 90˚E) for winters (December – February) from 1979/1980 to 2010/2011

The contour intervals are (a) 5 m, (b) 0.4 hPa, and (c) 0.2˚C. Warm- (cold-) color contours indicate negative (positive) values. The gray shading indicates a 90% confidence level as indicated by t-testing. COBE-SST sea ice concentration data were used for this analysis.

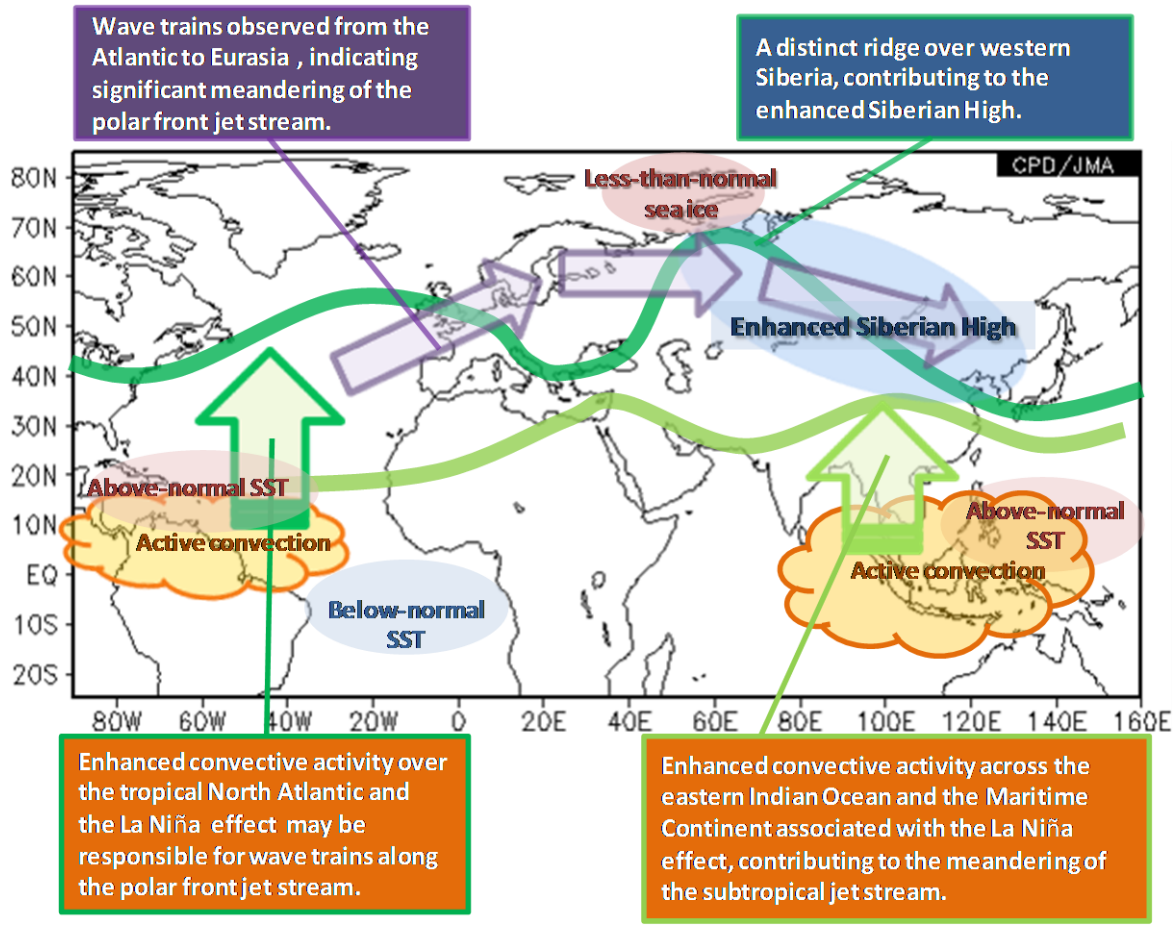

Figure 4.1 Primary factors contributing to the cold winter conditions of 2011/2012 in Central and East Asia